Effects of anisotropy on the stability of Giesekus fluid flow

Cite as: Phys. Fluids **34**, 124109 (2022); https://doi.org/10.1063/5.0125989
Submitted: 14 September 2022 • Accepted: 22 November 2022 • Accepted Manuscript Online: 23 November 2022 • Published Online: 09 December 2022

L. J. S. Furlan, M. T. Araujo, M. T. Mendonca, et al.

Physics of Fluids ARTICLE scitation.org/journal/phf

Effects of anisotropy on the stability of Giesekus fluid flow

Cite as: Phys. Fluids **34**, 124109 (2022); doi: 10.1063/5.0125989
Submitted: 14 September 2022 · Accepted: 22 November 2022 ·
Published Online: 9 December 2022

L. J. S. Furlan,[1] M. T. Araujo,[1] M. T. Mendonca,[2] A. C. Brandi,[3] and L. F. Souza[1,a)]

AFFILIATIONS

[1]Department of Applied Mathematics and Statistics, University of Sao Paulo, Sao Carlos, Sao Paulo, CEP 13566-590, Brazil
[2]Combustion and Propulsion Laboratory, National Institute for Space Research, Cachoeira Paulista, Sao Paulo, CEP 12630-000, Brazil
[3]Department of Mathematics and Computer Science, Sao Paulo State University, Presidente Prudente, Sao Paulo, CEP 19060-900, Brazil

Note: This paper is part of the special topic, One Hundred Years of Giesekus.
[a)]**Author to whom correspondence should be addressed:** lefraso@icmc.usp.br

ABSTRACT

In the present work, the stability of a viscoelastic fluid flow is studied by linear stability theory, and some results are verified by direct numerical simulation. The investigation considers the fluid flow between two parallel plates, modeled by the Giesekus constitutive equation. The results show the influence of the anisotropic tensorial correction parameter α_G on this model, showing a stabilizing influence for two-dimensional disturbances for small values of α_G. However, as α_G increases, a reduction in the critical Reynolds number values is observed, possibly hastening the transition to turbulence. Low values for α_G for three-dimensional disturbances cause more significant variations for the critical Reynolds number. This variation decreases as the value of this parameter increases. The results also show that low values of α_G increase the instability of three-dimensional disturbances and confirm that Squire's theorem is not valid for this model. As for the two-dimensional disturbances, the anisotropic term on the Giesekus model lowers the critical Reynolds number for higher quantities of polymer viscosity in the mixture and high values for the Weissenberg number.

I. INTRODUCTION

Polymers are increasingly replacing other materials. Therefore, products that use polymers should have satisfactory mechanical performance for a given application. In this sense, with the development of computer technology, there is a great interest in working with numerical simulations of these industrial applications and developing efficient numerical methods to simulate viscoelastic fluid flows. This requires a smaller financial investment compared to experiments in laboratories. These materials exhibit viscous and elastic properties simultaneously. They present complex molecules and high molar mass (long and structured molecules). Therefore, the classical Navier–Stokes equations cannot describe the flow dynamics of this type of material, and additional constitutive equations are required for the stress field, resulting in additional unknowns.

Maxwell's model[1,2] was one of the first attempts to describe the effect of the viscoelasticity of a given fluid. This model incorporates the idea of a fluid that exhibits characteristics of a Hookean elastic solid and Newtonian viscous fluid. The Oldroyd-B model[2–5] derives from the kinetic theory for concentrated and molten polymer solutions.[6] The polymer chain is represented by a set of two spheres linked by a spring. In this configuration, the spheres represent the system's center of mass. They are related to the hydrodynamic interaction between the solvent and the polymeric solution's macromolecules (the solvent's viscous drag force on the molecules). The springs represent the elasticity effect of the macromolecules or the restorative effect of the polymer. This ball/spring configuration called "*dumbbell*" is simplified by assuming a linear spring or Hooke spring behavior. The Oldroyd-B model can represent certain fluids with ideal elasticity, also known as "Boger" fluids.

The rheological model called the Giesekus model[7–9] is also based on molecular considerations with ball/spring systems where the spring follows Hooke's law. For the Giesekus model, a non-isotropy effect was introduced in defining the drag force on the spheres. This model results in equations with the form analogous to the UCM and Oldroyd-B models but containing nonlinear terms given by the products between the stress tensor components.

For any fluid flow, the transition to turbulence can be generalized as the result of the amplification of disturbances that may be present. The mathematical explanation for the occurrence of instabilities in Newtonian flows is a direct consequence of the nonlinear convective term in the momentum equation. However, in viscoelastic flows, the nonlinearities emerge through convection terms in the momentum equation and in the extra-stress tensor equation. Draad *et al.*[10] reported a transition delay for viscoelastic fluid flows; the onset was postponed to a higher Reynolds number than Newtonian fluid flows. In another study, Ram and Tamir[11] observed that turbulence sets in at a Reynolds number smaller than in the Newtonian case, a phenomenon called "early turbulence." It has recently been demonstrated that at a large Weissenberg number, the anisotropic elastic stresses destabilize flows with curved streamlines even in the absence of inertia, resulting in so-called "purely elastic linear instabilities."[12] It is clear that the instability for viscoelastic fluid flows is not only inertial since it may exist at a zero Reynolds number.[13]

Several purely elastic instabilities have been reported in recent years corresponding to experimental or theoretical work using linear stability analysis.[14–19] In most works on this type of analysis in viscoelastic flows, the UCM and Oldroyd-B constitutive models have been employed. The constitutive model choice directly affects the stability analysis results. For example, the Oldroyd-B model shows more stabilization than the UCM model in a parallel flow when the solvent viscosity is taken into account.[20] Therefore, several works in the literature perform the stability analysis for other types of viscoelastic models, geometries, and fluid flow types.[21–26] Even today, studies in parallel flows have not been widely developed, and some questions still need to be answered, especially in viscoelastic fluid stability. Furlan *et al.*[27] presented theoretical results regarding the influence of the molecular composition of viscoelastic fluids and its relation to the stability of these fluids. Viscoelastic models with anisotropic terms, such as Giesekus, LPTT, and FENE-type models, do not satisfy Squire's theorem.[27] Therefore, three-dimensional disturbances may have a stronger destabilizing effect than two-dimensional ones.

This work presents numerical results for the stability analysis of 2D and 3D disturbances in viscoelastic fluid flows between two parallel plates. The Giesekus constitutive equation is used to model the fluid. Linear stability theory (LST) has been used to analyze the stability of an incompressible parallel flow of a viscoelastic fluid. The stability problem is solved using a system of linearized equations, rewriting in an eigenvalue problem solved through the matrix method. Different viscoelastic fluid characteristics are considered, such as the fraction of polymer viscosity in the mixture, the mobility parameter that regulates the fluid's shear thinning behavior and different values of the Weissenberg number (ratio of elastic and viscous forces). The adopted baseflow is 2D, although the stability of 2D and 3D disturbances are analyzed, assuming periodicity in the spanwise direction. The fact that Squire's theorem is not valid is observed through the LST analyses, and direct numerical simulation (DNS) results double-check some results.[28]

Previous investigations on the stability of non-Newtonian flows based on the Giesekus model indicate the need to investigate flow instability to three-dimensional disturbances due to anisotropy.[22,27,29,30] In the present work, the effects of the mobility parameter α_G on the stability of the planar Poiseuille flow are investigated and how these effects change when the other parameters (Wi, β, and spanwise wavelength γ) change. The results will show that three-dimensional disturbances can be more unstable than two-dimensional, as previously suspected but not quantified.

This work is organized as follows: Sec. II presents the governing equations, the linear stability equations, and the solution method. Section III shows the results obtained for the linear stability analysis for two- and three-dimensional disturbances. The main conclusions are presented in Sec. IV.

II. MATHEMATICAL FORMULATION

Incompressible and isothermal flows in dimensionless form for viscoelastic fluids can be governed by the mass conservation equation

$$\nabla \cdot \mathbf{u} = 0, \tag{1}$$

and by the momentum equation

$$\frac{\partial \mathbf{u}}{\partial t} + \nabla \cdot (\mathbf{uu}) = -\nabla p\mathbf{I} + \frac{\beta}{Re}\nabla^2\mathbf{u} + \nabla \cdot \mathbf{T}, \tag{2}$$

where p is the pressure, $\mathbf{u}$ is the velocity field, t is the time, and $\beta = \eta_s/\eta_0$ is the coefficient that controls the solvent viscosity contribution ($\eta_0 = \eta_s + \eta_p$), where η_s and η_p are the solvent and the polymer viscosity, respectively. $Re = (\rho UL)/\eta_0$ is the Reynolds number, ρ is the fluid density, L is the length scale (for the channel flow is the channel half-width in the y direction), U is the velocity scale, and $\mathbf{T}$ is the symmetric non-Newtonian extra-stress tensor. The velocity $U = 1$ is adopted for the non-dimensionalization. The same flow rate for the Newtonian flow ($\int_{-1}^{1} udy = 4/3$) is adopted in the baseflow solution.[31] The viscoelastic constitutive equation for the Giesekus model[8] is given by

$$\mathbf{T} + Wi\left(\frac{\partial \mathbf{T}}{\partial t} + \nabla \cdot (\mathbf{uT}) - \nabla\mathbf{u} \cdot \mathbf{T} - \mathbf{T} \cdot \nabla\mathbf{u}^T\right) + \frac{\alpha_G Re Wi}{(1-\beta)}(\mathbf{T} \cdot \mathbf{T}) = 2\frac{(1-\beta)}{Re}\mathbf{D}, \tag{3}$$

where $\mathbf{D} = (1/2)(\nabla\mathbf{u} + (\nabla\mathbf{u})^T)$ is the rate of deformation tensor, $Wi = \lambda U/L$ is the Weissenberg number, and λ is the relaxation time of the fluid. The α_G represents the mobility parameter that regulates the fluid's shear thinning behavior and the amplitude of anisotropy, with $\alpha_G = 1$ denoting maximum anisotropy and $\alpha_G = 0$ denoting the original isotropic relaxation in the UCM model.[32] The terms with α_G can be associated with the anisotropic hydrodynamic drag on the constituent polymer molecules.[6]

Figure 1 illustrates the computational domain. The 2D-baseflow adopted is a fully developed flow, and it is obtained by a semi-analytical solution.[31] The baseflow solution is obtained for each combination of fluid and flow parameters. The main flow direction is in the x direction, the flow is confined between two parallel plates placed in fixed y positions, and periodicity is adopted in the spanwise direction z.

A. Linear stability theory

It is assumed that the instantaneous flow can be decomposed into laminar and disturbance components. Adopting u, v, and w as velocity components in the x, y, and z directions, respectively, the variables can be decomposed as follows:

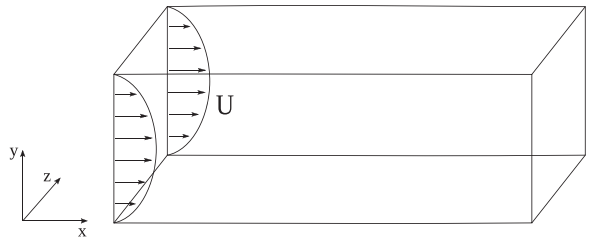

FIG. 1. Computational domain.

$$u(x,y,z,t) = U(y) + \tilde{u}(x,y,z,t),$$
$$v(x,y,z,t) = \tilde{v}(x,y,z,t),$$
$$w(x,y,z,t) = \tilde{w}(x,y,z,t),$$
$$p(x,y,z,t) = P(x,y) + \tilde{p}(x,y,z,t),$$

and the non-Newtonian extra-stress tensors components can be decomposed as

$$T(x,y,z,t) = Tb(y) + \tilde{T}(x,y,z,t),$$

where the components of the laminar flow (baseflow) are $U(y)$, $P(x, y)$, and $Tb(y)$. The components of the disturbed flow (disturbances) are represented with a superscript $\sim$. The non-Newtonian tensor components Tb_{xz}, Tb_{yz}, and Tb_{zz} are zero for the baseflow. Figure 2 presents an example of a baseflow result considering $Re = 3400$, $\beta = 0.5$, $\alpha_G = 0.1$, and $Wi = 6$. The maximum streamwise velocity component is below 1, but the flow rate is the same as that of the Newtonian fluid flow ($\int_{-1}^{1} u dy = 4/3$). The extra tensor components T_{xx}, T_{xy}, and T_{yy} are normalized by each maximum absolute value, 4.66×10^{-04}, 5.38×10^{-05}, and 1.24×10^{-05}, respectively. The derivative of this velocity component in the wall-normal direction, also normalized by its maximum absolute value, is shown. The Giesekus fluid parameters significantly influence the baseflow, and the solution shown in Fig. 2 is only an example. Baseflow examples and the influence of each parameter can be found in Furlan *et al.*[31]

The baseflow is assumed steady (does not change in time) and constant in the x and z directions. By the continuity equation, the normal-wall component of the mean velocity is zero (the flow is locally parallel). The baseflow was obtained using the solution form presented by Furlan *et al.*[31] Substituting this decomposition into the equations and subtracting from the resulting equations, the equations satisfied by the laminar flow, and we obtain the linear equations with coefficients not depending on t, x, and z. Therefore, a solution in terms of normal modes may be sought for the disturbances $\tilde{u}$, $\tilde{v}$, $\tilde{w}$, $\tilde{p}$, and $\tilde{T}$. Rewriting the system of equations for the flow disturbances using the solutions obtained by normal mode decomposition

$$\tilde{u}(x,y,z,t) = \frac{1}{2}\left[\bar{u}(y)e^{i(\alpha x+\gamma z-\omega_t t)} + cc.\right],$$
$$\tilde{v}(x,y,z,t) = \frac{1}{2}\left[\bar{v}(y)e^{i(\alpha x+\gamma z-\omega_t t)} + cc.\right],$$
$$\tilde{w}(x,y,z,t) = \frac{1}{2}\left[\bar{w}(y)e^{i(\alpha x+\gamma z-\omega_t t)} + cc.\right],$$
$$\tilde{p}(x,y,z,t) = \frac{1}{2}\left[\bar{p}(y)e^{i(\alpha x+\gamma z-\omega_t t)} + cc.\right],$$
$$\tilde{T}(x,y,z,t) = \frac{1}{2}\left[\bar{T}(y)e^{i(\alpha x+\gamma z-\omega_t t)} + cc.\right],$$

where the variables with overbar are the amplitude in each y position, and $cc.$ is the complex conjugate. Removing the overbar for simplicity and simplifying, Eq. (1) can be rewritten as

$$i\alpha u + i\gamma w + \frac{dv}{dy} = 0, \tag{4}$$

the momentum equation—Eq. (2), in each direction, can be given as

$$-i\omega_t u + iU\alpha u + v\frac{dU}{dy} = -i\alpha p + \frac{\beta}{Re}\left(-(\alpha^2+\gamma^2)u + \frac{d^2u}{dy^2}\right) + i\alpha T_{xx} + \frac{dT_{xy}}{dy} + i\gamma T_{xz}, \tag{5}$$

$$-i\omega_t v + iU\alpha v = -\frac{dp}{dy} + \frac{\beta}{Re}\left(-(\alpha^2+\gamma^2)v + \frac{d^2v}{dy^2}\right) + i\alpha T_{xy} + \frac{dT_{yy}}{dy} + i\gamma T_{yz}, \tag{6}$$

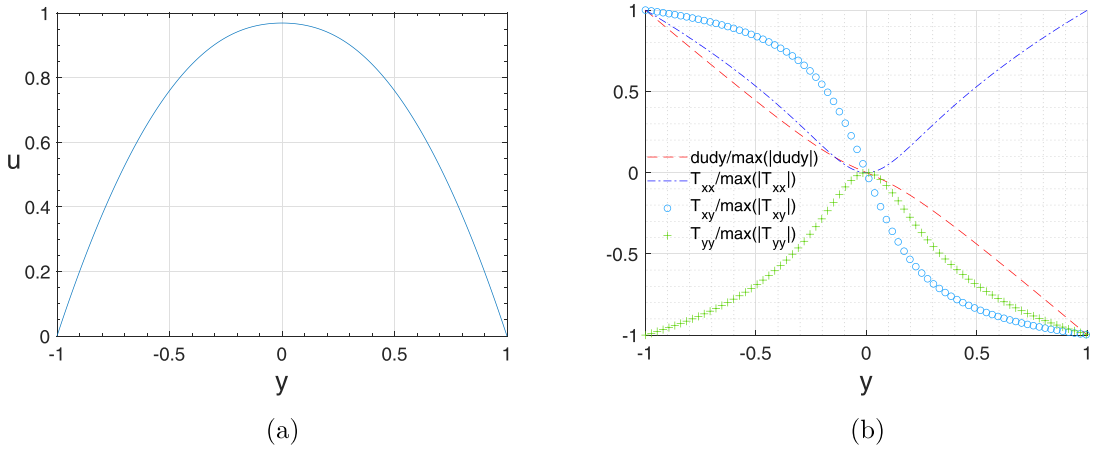

(a) (b)

FIG. 2. Baseflow components for $Re = 3400$, $\beta = 0.5$, $\alpha_G = 0.1$, and $Wi = 6$. (a) Streamwise velocity component u. (b) $dudy$, and tensor component profile.

TABLE I. Comparison between the wave velocities presented in Blonce[22] and the results obtained in this work. The results of the present work were performed using 150 Chebyshev modes.

β	α_G	Re	Wi	ω_t	Blonce α_r	LST α
0.2	0.1	5489.34	4.720 832 4	0.207 149 60	1.0420	1.044 79 − 0.000 185 2i
	0.3	4064.09	3.495 117 4	0.222 186 04	1.0636	1.063 30 + 0.000 065 2i
	0.5	3593.21	3.090 160 6	0.229 959 84	1.0776	1.077 50 + 0.000 081 4i
0.5	0.1	4944.61	4.252 364 6	0.236 887 20	0.9970	1.001 25 − 0.000 044 3i
	0.3	4271.79	3.673 739 4	0.244 079 86	1.0061	1.005 99 + 0.000 002 1i
	0.5	4070.37	3.500 518 2	0.251 057 88	1.0107	1.020 64 − 0.000 436 2i
0.8	0.1	5350.89	4.601 765 4	0.259 226 70	1.013	1.012 98 + 0.000 014 9i
	0.3	5092.37	4.379 438 2	0.264 117 04	1.0174	1.020 31 − 0.000 031 3i
	0.5	4980.98	4.283 642 8	0.264 454 52	1.0187	1.018 53 + 0.000 011 4i

$$-i\omega_t w + iU\alpha w = -i\gamma p + \frac{\beta}{Re}\left(-(\alpha^2+\gamma^2)w + \frac{d^2w}{dy^2}\right) + i\alpha T_{xz} + \frac{dT_{yz}}{dy} + i\gamma T_{zz}, \tag{7}$$

and the components of the extra stress tensor, Eq. (3), can be given as

$$T_{xx} + Wi\left(-i\omega_t T_{xx} + i\alpha U T_{xx} - 2i\alpha T b_{xx} u + \frac{dTb_{xx}}{dy}v - 2\frac{dU}{dy}T_{xy} - 2Tb_{xy}\frac{du}{dy}\right) + \frac{2\alpha_G WiRe}{(1-\beta)}(Tb_{xx}T_{xx} + Tb_{xy}T_{xy}) = \frac{2i\alpha(1-\beta)}{Re}u, \tag{8}$$

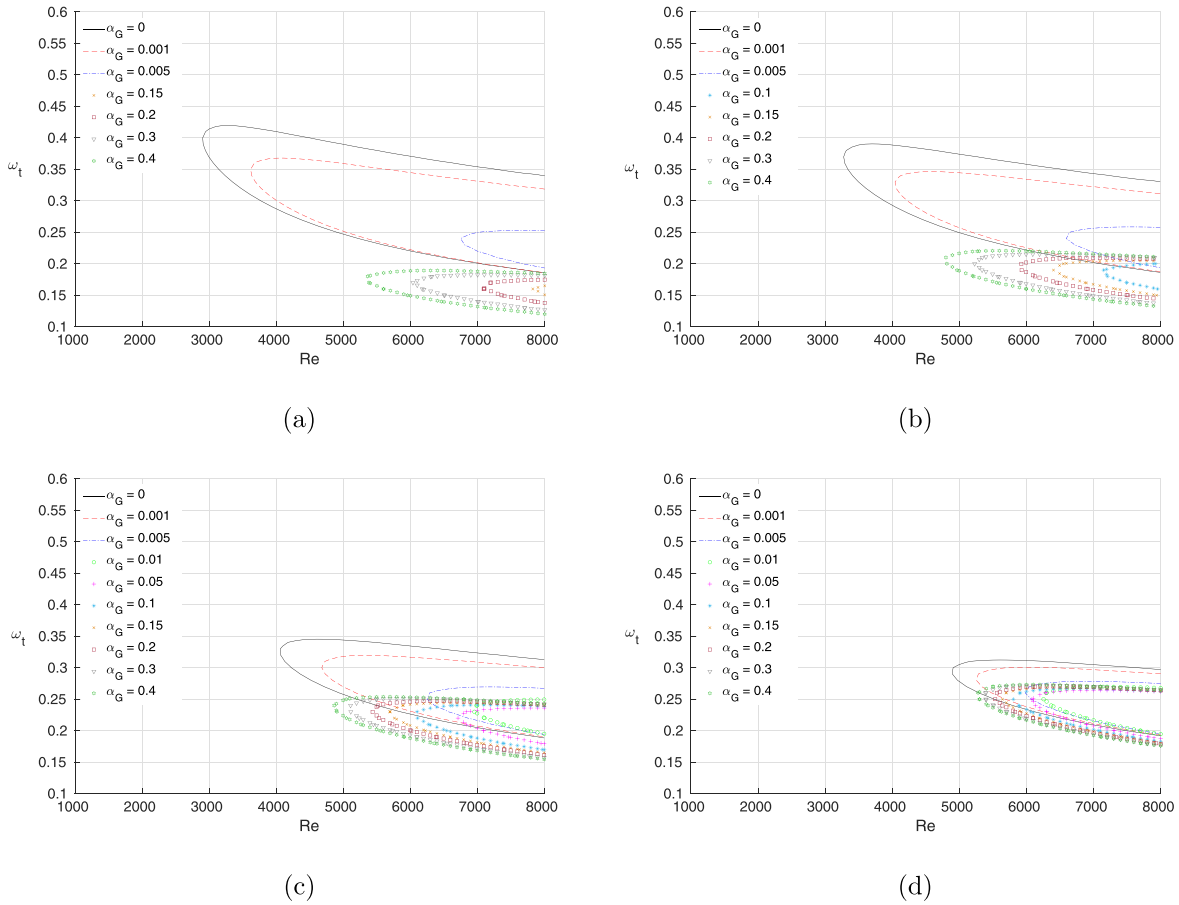

FIG. 3. Neutral curves for two-dimensional disturbances for different values of α_G considering $Wi = 2$, for (a) $\beta = 0.125$, (b) $\beta = 0.25$, (c) $\beta = 0.5$, and (d) $\beta = 0.75$.

$$T_{xy} + Wi\Big(-i\omega_t T_{xy} + i\alpha U T_{xy} - i\alpha T b_{xx} v + i\gamma T b_{xy} w + \frac{dTb_{xy}}{dy} v - \frac{dU}{dy} T_{yy} - Tb_{yy}\frac{du}{dy}\Big) + \frac{\alpha_G WiRe}{(1-\beta)}\left[Tb_{xy}(T_{xx}+T_{yy}) + T_{xy}(Tb_{xx}+Tb_{yy})\right] = \frac{(1-\beta)}{Re}\left(\frac{du}{dy} + i\alpha v\right), \quad (9)$$

$$T_{xz} + Wi\Big(-i\omega_t T_{xz} + i\alpha U T_{xz} - i\alpha T b_{xx} w - Tb_{xy}\frac{dw}{dy} + -\frac{dU}{dy} T_{yz}\Big) + \frac{\alpha_G WiRe}{(1-\beta)}(Tb_{xx}T_{xz} + Tb_{xy}T_{yz}) = \frac{(1-\beta)}{Re}(i\gamma u + i\alpha w), \quad (10)$$

$$T_{yy} + Wi\Big(-i\omega_t T_{yy} + i\alpha U T_{yy} + \frac{dTb_{yy}}{dy} v - 2i\alpha T b_{xy} v - 2Tb_{yy}\frac{dv}{dy}\Big) + \frac{2\alpha_G WiRe}{(1-\beta)}(Tb_{xy}T_{xy} + Tb_{yy}T_{yy}) = \frac{2(1-\beta)}{Re}\frac{dv}{dy}, \quad (11)$$

$$T_{yz} + Wi\Big(-i\omega_t T_{yz} + i\alpha U T_{yz} - i\alpha T b_{xy} w - Tb_{yy}\frac{dw}{dy}\Big) + \frac{\alpha_G WiRe}{(1-\beta)}(Tb_{xy}T_{xz} + Tb_{yy}T_{yz}) = \frac{(1-\beta)}{Re}\left(\frac{dw}{dy} + i\gamma v\right), \quad (12)$$

$$T_{zz} + Wi(-i\omega_t T_{zz} + i\alpha U T_{zz}) = \frac{2i\gamma(1-\beta)}{Re} w, \quad (13)$$

with $i = \sqrt{-1}$.

These equations indicate that the disturbances propagate as waves, with frequency ω_t, wavelength $\Lambda_x = 2\pi/\alpha$, and $\Lambda_z = 2\pi/\gamma$. The wave speed can be given as $c = \omega_t/\alpha$, with α being the wavenumber in the x direction and γ the wavenumber in the z direction, and the respective amplitudes u, v, w, p, and T.

B. Solution method

The stability analysis is performed by obtaining the solution of the system of equations (4)–(13). The system of equations is written in matrix form, and the stability analysis problem becomes an eigenvalue/eigenvector problem. In the present work, the spatial analysis of the disturbances was performed where the amplification rate α_i is analyzed. Rewriting the system of equations in matrix form as

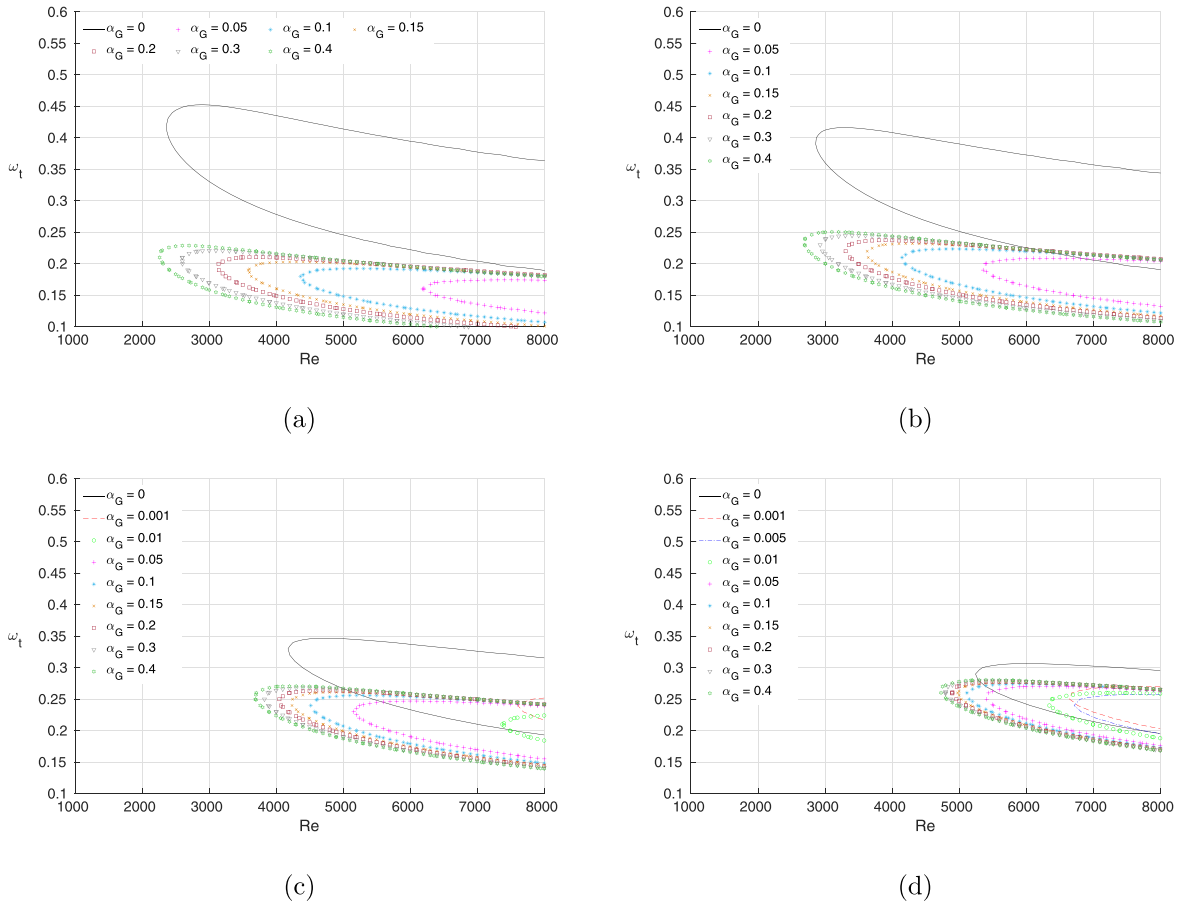

FIG. 4. Neutral curves for two-dimensional disturbances for different values of α_G considering $Wi = 6$, for (a) $\beta = 0.125$, (b) $\beta = 0.25$, (c) $\beta = 0.5$, and (d) $\beta = 0.75$.

$$LV = \alpha FV, \tag{14}$$

for the eigenvector V,

$$V = [u, \alpha u, v, \alpha v, w, \alpha w, p, T_{xx}, T_{xy}, T_{xz}, T_{yy}, T_{yz}, T_{zz}]. \tag{15}$$

It is possible to solve the stability analysis problem by finding the eigenvalue α (or ω_t for the time analysis), using a method (direct or iterative) for calculating the eigenvalue.

The y-direction derivatives are approximated using Chebyshev polynomials.[33,34] These polynomials are related to the cosine and sine functions; therefore, the derivative calculations are found easily, with the advantage of low discretization errors. Details about the matrices L and F, their coefficients, and the boundary conditions are presented in the Appendix.

C. Spatial and temporal analysis of instabilities

The solution of the system (14) corresponds to an eigenvalue problem, whose solution exists for some values of the parameters α, ω_t, γ, Re, β, Wi, and α_G, and depends on the velocity profile of the flow. The disturbances analyzed here are non-stationary and propagate as Tollmien–Schlichting waves.

When ω_t is a real number, and α is a complex number, the amplitude of the disturbance can increase, decrease, or be neutral in the direction of the laminar flow. Under these conditions, the formulation is called a spatial formulation. The components ω_t, α_r, and α_i represent the frequency, the wavenumber, and the spatial amplification rate, respectively. For the temporal formulation, α is a real number, and ω_t is a complex number. The components ω_r, ω_i, and α represent the frequency, the temporal amplification rate, and the wavenumber, respectively.

III. RESULTS

This section presents the results obtained for the stability analysis of flows considering the Giesekus viscoelastic model. The neutral stability curves (stability diagram) were built considering the Reynolds number on the horizontal axis and the angular frequency ω_t on the vertical axis.

A. Two-dimensional disturbances analysis

1. Verification

In order to verify the numerical model, Table I presents comparisons between the results presented by Blonce[22] for the stability analysis

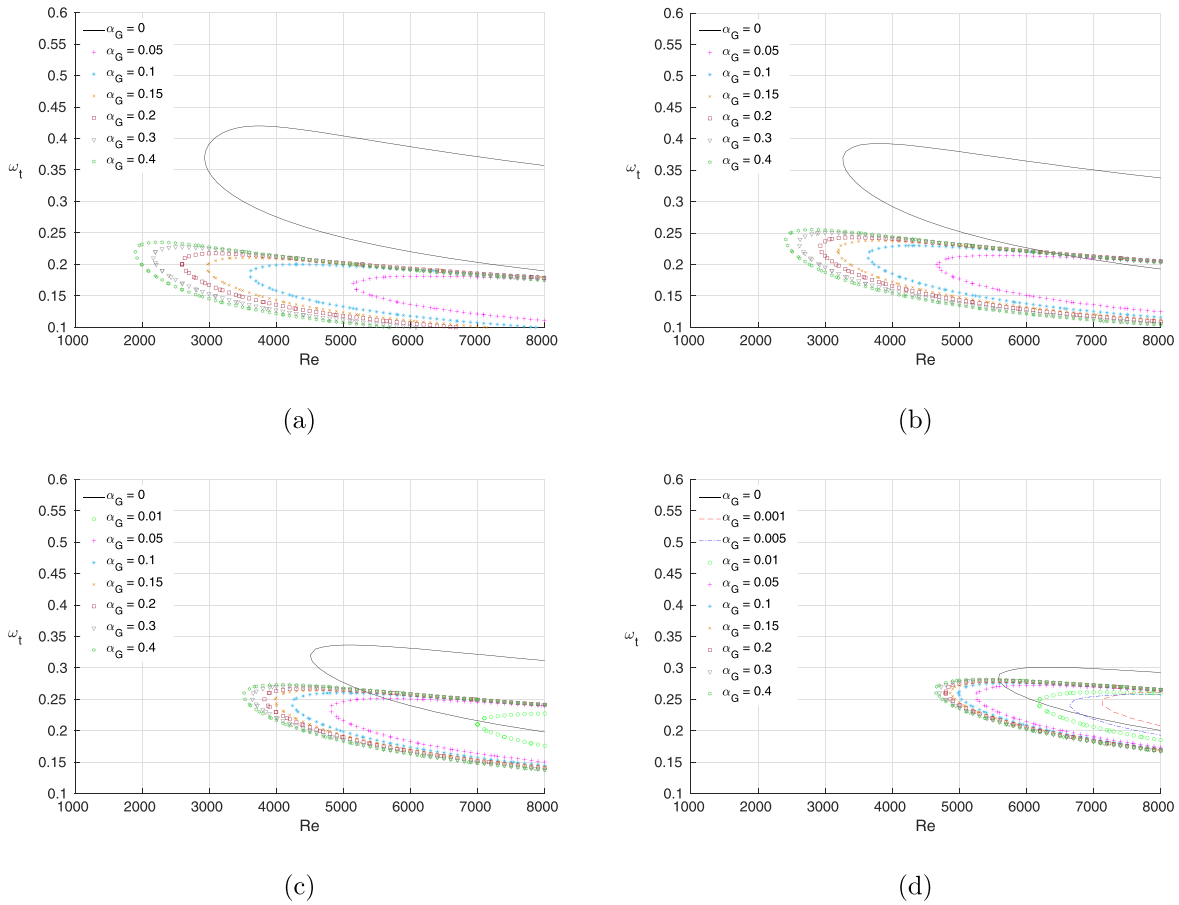

FIG. 5. Neutral curves for two-dimensional disturbances for different values of α_G considering $Wi = 8$, for (a) $\beta = 0.125$, (b) $\beta = 0.25$, (c) $\beta = 0.5$, and (d) $\beta = 0.75$.

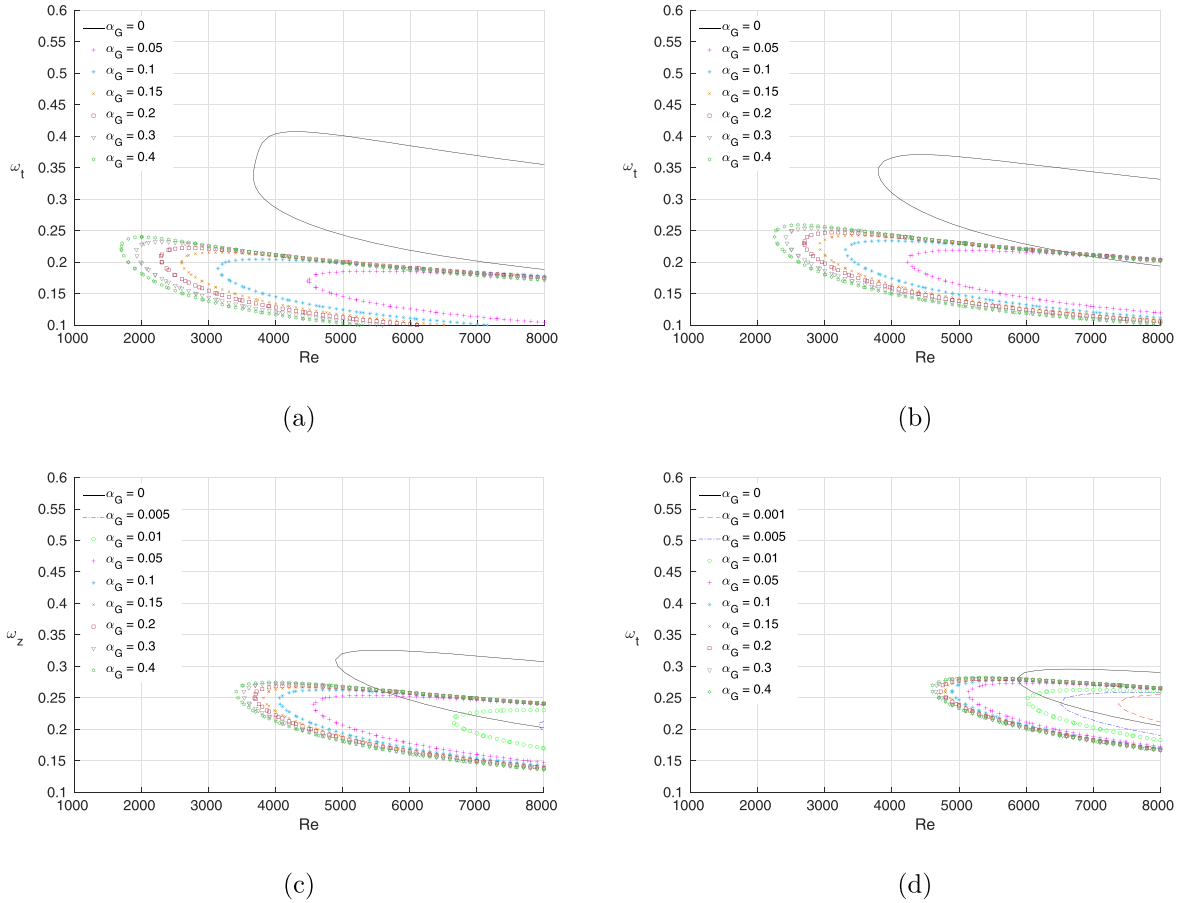

FIG. 6. Neutral curves for two-dimensional disturbances for different values of α_G considering $Wi = 10$, for (a) $\beta = 0.125$, (b) $\beta = 0.25$, (c) $\beta = 0.5$, and (d) $\beta = 0.75$.

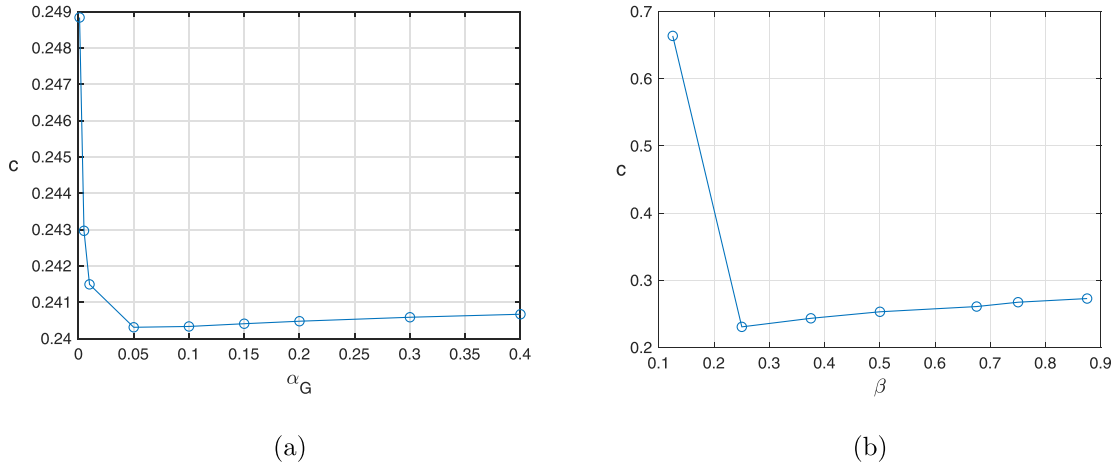

FIG. 7. Wave Speed variation with α_g and β. (a) Wave velocity variation with α_G for $Re = 2500$, $\beta = 0.5$, $\omega_t = 0.2$, and $Wi = 6.0$. (b) Wave velocity variation with β for $Re = 5000$, $\alpha_G = 0.1$, $\omega_t = 0.3$, and $Wi = 10.0$.

TABLE II. Comparison between the amplification rates obtained with the LST and DNS techniques. The results of the present work were performed using 150 Chebyshev modes.

β	α_G	Re	Wi	ω_t	γ	α_r	α_i − LST	α_i − DNS
0.25	0.005	12 000	8	0.13	0	0.785 534 1	0.004 189 69	0.004 266 69
0.25	0.005	12 000	8	0.13	0.8	0.602 071 8	−0.010 264 97	−0.010 559 78
0.50	0.1	3400	6	0.29	0.1	1.099 696 4	0.010 294 14	0.010 420 72
0.50	0.1	3400	6	0.29	0.8	0.987 494 4	0.025 568 69	0.025 545 35
0.50	0.15	7300	8	0.20	0.2	0.925 387 02	−0.013 519 77	−0.013 497 73
0.75	0.4	4700	8	0.27	1.2	0.820 487 32	0.060 347 85	0.060 122 40

of the Giesekus model flow with the results obtained using the present method. This comparison is performed using a neutral growth rate $\alpha_i = 0$ (i.e., values at the neutral stability curve), obtained by solving the system (14). Blonce[22] uses different variables than the one used in this paper, such as the parameter E, written as $E = Wi/Re$, and the equations for the disturbances wave velocity c are used. To verify the results presented in this work, the value of $E = 8.6 \times 10^{-4}$ was adopted.

2. Two-dimensional stability analysis

The parameter α_G of the Giesekus model influences two- and three-dimensional disturbances. Therefore, it is necessary to analyze the influence of this parameter under both types of disturbances. For two-dimensional disturbances, a variation of this parameter was performed considering different values of β and the Weissenberg number

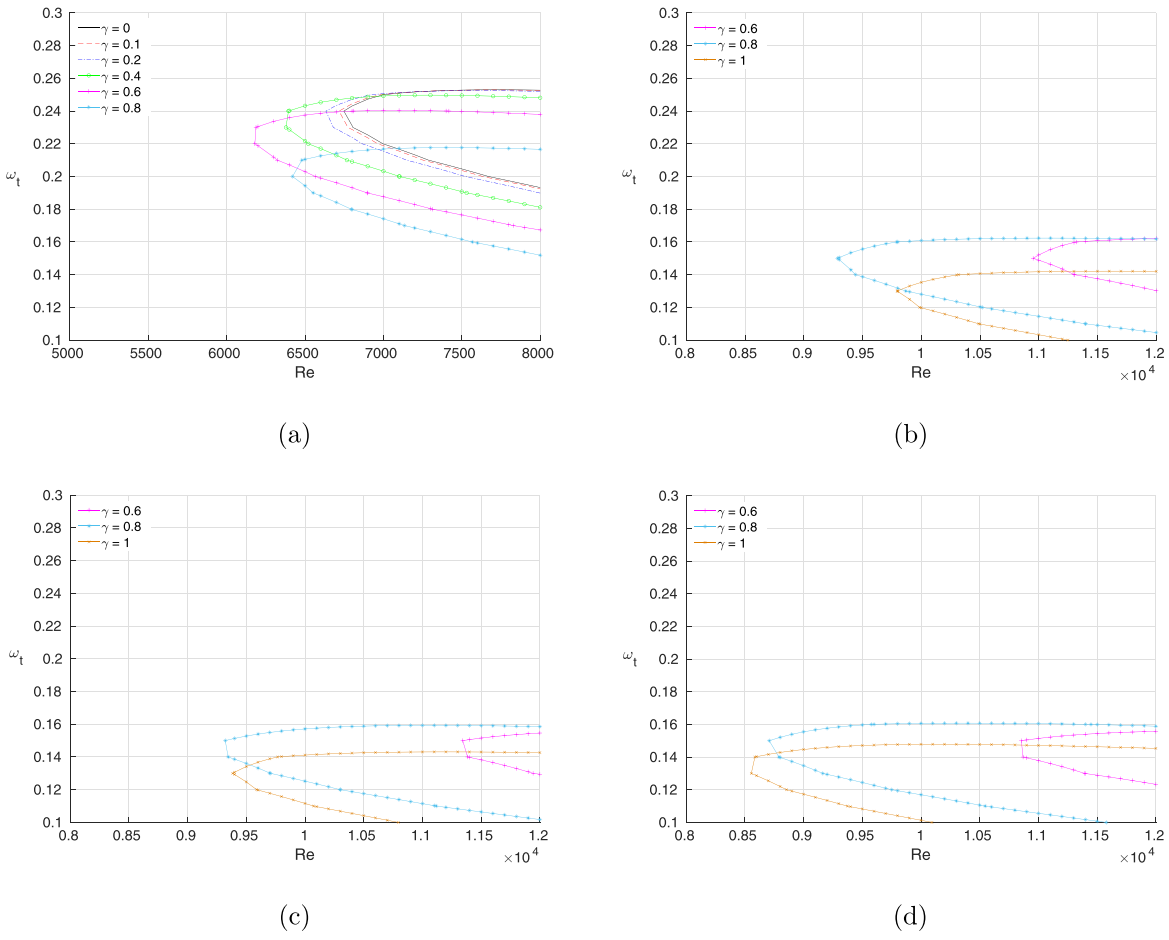

FIG. 8. Neutral curves for three-dimensional disturbances for different values of γ considering $\beta = 0.125$ and $\alpha_G = 0.005$, for (a) $Wi = 2$, (b) $Wi = 6$, (c) $Wi = 8$, and (d) $Wi = 10$.

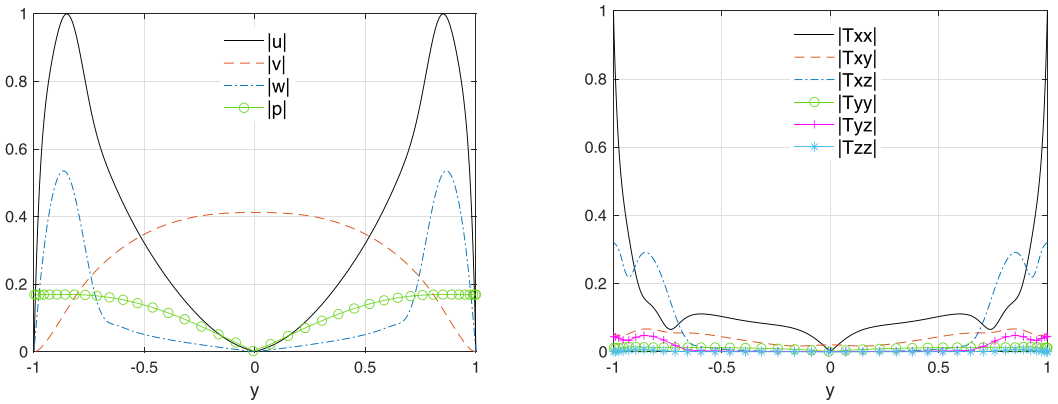

FIG. 9. Eigenfunctions for $\beta = 0.50$, $\alpha_G = 0.1$, $Re = 3400$, $Wi = 6$, $\omega_t = 0.29$, $\gamma = 0.8$, and $\alpha_i = 0.025\,568\,69$. (a) Velocity components and the pressure. (b) Extra stress tensor components.

in order to analyze its influence under many different conditions and flow characteristics.

Figure 3 presents the neutral stability curves for two-dimensional disturbances by varying the values of the parameter α_G, considering $Wi = 2$, and $\beta = 0.125, 0.25, 0.5$, and 0.75.

It is possible to observe that the parameter α_G, for these cases, acts as a stabilizing factor in the flow for low values of α_G. As α_G increases, the instability region starts to grow. In the plots where the curves do not appear, the stabilization was so high that the critical Reynolds is higher than 8000. As the percentage of solvent viscosity contribution increases in the fluid mixture ($\beta \to 1$), this stabilizing effect becomes smaller, to the point that the neutral curves for $\beta = 0.75$ do not show significant differences between the Oldroyd-B fluid ($\alpha_G = 0$) and the Giesekus fluid.

An interesting behavior in these results is how the neutral curve decreases in size (increasing the critical Reynolds) and then increases again (decreasing the critical Reynolds) as the parameter α_G increases. This behavior is more pronounced when we look at the neutral curves considering smaller values for β, that is, the most significant non-Newtonian contribution in the fluid mixture (about 87.5%). As the Newtonian contribution increases in the fluid mixture with increasing β, this behavior reduces, as shown in Fig. 3(d).

As the α_G parameter is related to the mobility of the fluid, it is interesting to analyze its influence as the elasticity of the fluid increases. Figure 4 presents the neutral stability curves for two-dimensional disturbances by varying the values of the parameter α_G, considering $Wi = 6$, and $\beta = 0.125, 0.25, 0.5$, and 0.75.

The parameter α_G stabilizing effect held for small values even with increasing Weissenberg. It can be observed that this effect was more substantial, as a slight increase in α_G ($0 \to 0.001$) caused the critical Reynolds to increase from $\approx$2500 to more than 8000 (considering the cases $\beta = 0.125$ and 0.25). It is also possible to observe that, as the value of the parameter α_G increases (values greater than 0.05), the critical Reynolds decreases to the point that for $\alpha_G = 0.4$, the critical Reynolds is smaller than that of the Oldroyd-B model.

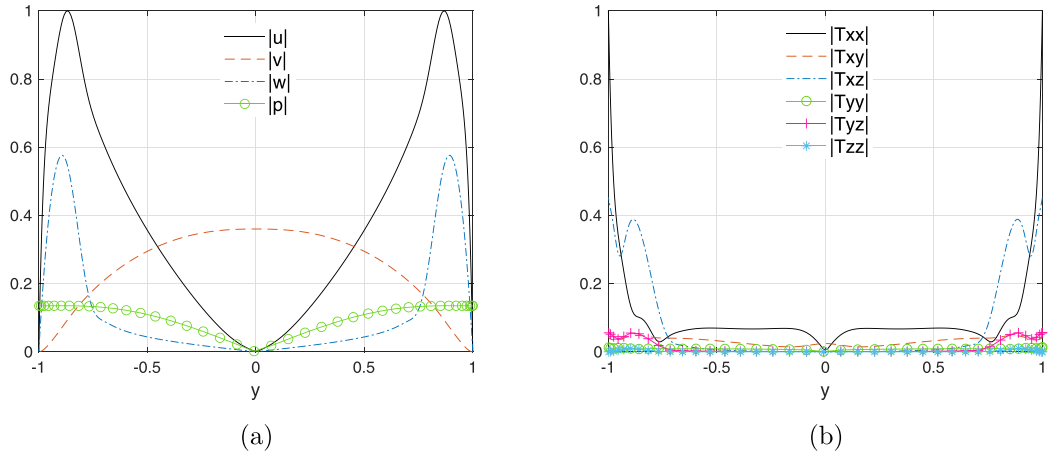

FIG. 10. Eigenfunctions for $\beta = 0.50$, $\alpha_G = 0.15$, $Re = 7300$, $Wi = 8$, $\omega_t = 0.20$, $\gamma = 0.2$, and $\alpha_i = -0.013\,519\,77$. (a) Velocity components and the pressure. (b) Extra-stress tensor components.

When the value of the Weissenberg number increases to 8, the behavior of the neutral stability curves can be observed in Fig. 5 for $\beta = 0.125, 0.25, 0.5$, and 0.75.

The critical Reynolds value decreases as the Weissenberg number increases for higher amounts of polymer viscosity in the mixture. When the amount of solvent viscosity in the mixture increases, this behavior is less pronounced since the amount of polymer viscosity is high. However, the increase in α_G continues to cause the instability regions to increase after a certain threshold. The results show the influence of α_G, which for low values is stabilizing, even considering higher values for the Weissenberg number. However, for higher values of this parameter, it is possible to observe that the destabilizing effect also increases.

The viscosity of the polymer has the effect of increasing the potential of the parameter α_G. The stabilizing and destabilizing effects are enhanced for high amounts of polymer in the mixture. As the amount of polymer in the fluid decreases, both effects decrease their power.

Figure 6 presents the neutral curves for the same values of α_G shown in the last figures, considering $Wi = 10$. The behavior exhibited by the influence of the parameter α_G holds for this value of the Weissenberg number.

Comparing the results from Figs. 3 and 6, the lower critical Reynolds numbers for higher Wi as α_G increases may be associated with both the increased influence of the anisotropic stress tensor components and shear thinning associated with higher α_G. The stabilizing effect of the high values of elastic forces ($Wi = 10$) and solvent viscosity effect (increasing β) is offset by the destabilizing effects of the anisotropic stress tensor and shear thinning for large values of α_G. This effect will be considered again for three-dimensional disturbances where, in addition, the anisotropic fluid properties are relevant to the amplification of oblique waves.

3. Wave speed analysis

Figure 7 analyzes the influence of the shear thinning parameter, α_G, and the amount of solvent in the mixture, β, on the wave speed $c = \omega_t/\alpha_r$. In Fig. 7(a), it can be seen that the phase velocity slightly increases after $\alpha_g = 0.05$, but for values lower than 0.05, a significant increase in the phase velocity is observed. However, the maximum

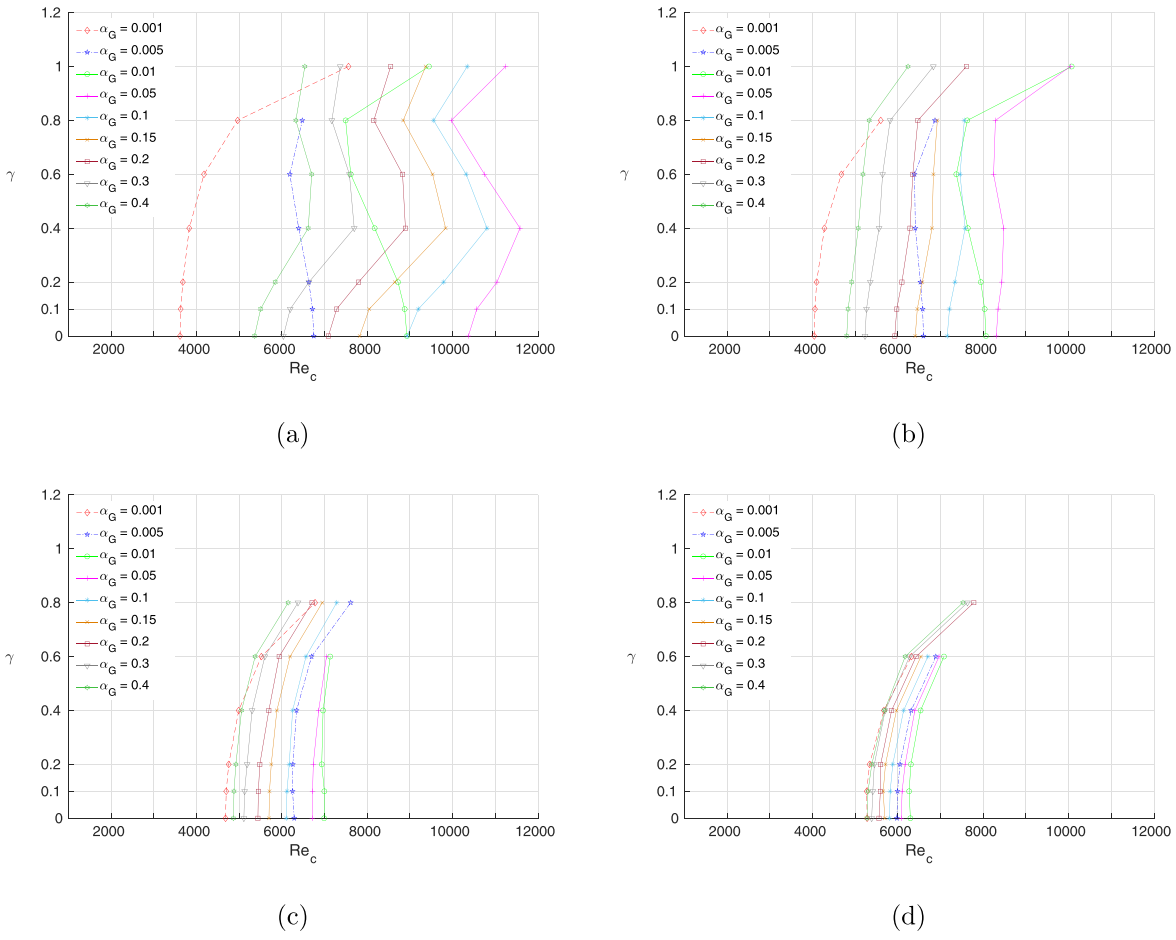

FIG. 11. Critical Reynolds number for three-dimensional disturbances for different values of β and α_G for $Wi = 2$, for (a) $\beta = 0.125$, (b) $\beta = 0.25$, (c) $\beta = 0.5$, and (d) $\beta = 0.75$.

difference observed in this graphic is around 0.09. The influence of β presented in Fig. 7(b) shows that after $\beta = 0.25$, the change in the phase velocity is small, but a more considerable increase can be observed for $\beta = 0.125$. The substantial variation observed on the neutral curves when α_G increases from zero to 0.05 is also observed for the wavenumber α_r and, consequently, on the wave speed, as observed in Fig. 7(a).

B. Three-dimensional disturbance analysis

As presented in Furlan *et al.*,[27] it is impossible to predict the behavior of three-dimensional disturbances by considering Squire's theorem for the Giesekus model. Therefore, it is necessary to perform a separate analysis for three-dimensional disturbances.

1. LST and DNS comparisons

Table II compares the LST results with DNS results[28] considering three-dimensional disturbances ($\gamma > 0$). Araujo[28] solved the stability problem for this same viscoelastic model using the DNS technique. The DNS code adopted[28] is based on vorticity–velocity formulation and is an extension of the 2D code adopted by Brandi *et al.*[26] The code uses compact finite differences for the streamwise and wall-normal directions and Fourier transforms in the spanwise direction for spatial discretizations.

Table II shows a good agreement between the results obtained by the two computational techniques for the stability analysis. This agreement assures the quality of the results obtained in this work considering three-dimensional disturbances.

The only change in the second line of Table II compared to the first line is that the spanwise wavenumber γ changes from 0 to 0.8. The α_i changes from a positive value to a negative one, showing that the three-dimensional disturbance is unstable while the two-dimensional one is stable. This proves the non-applicability of the Squire theorem for this fluid model. This behavior is also illustrated in Fig. 8, for $Wi = 2$, $Wi = 6$, $Wi = 8$, and $Wi = 10$. This figure shows neutral stability curves for different values for the spanwise wavenumber γ.

Figure 8 shows that increasing the Weissenberg number stabilizes two-dimensional disturbances. This effect is so strong that, from

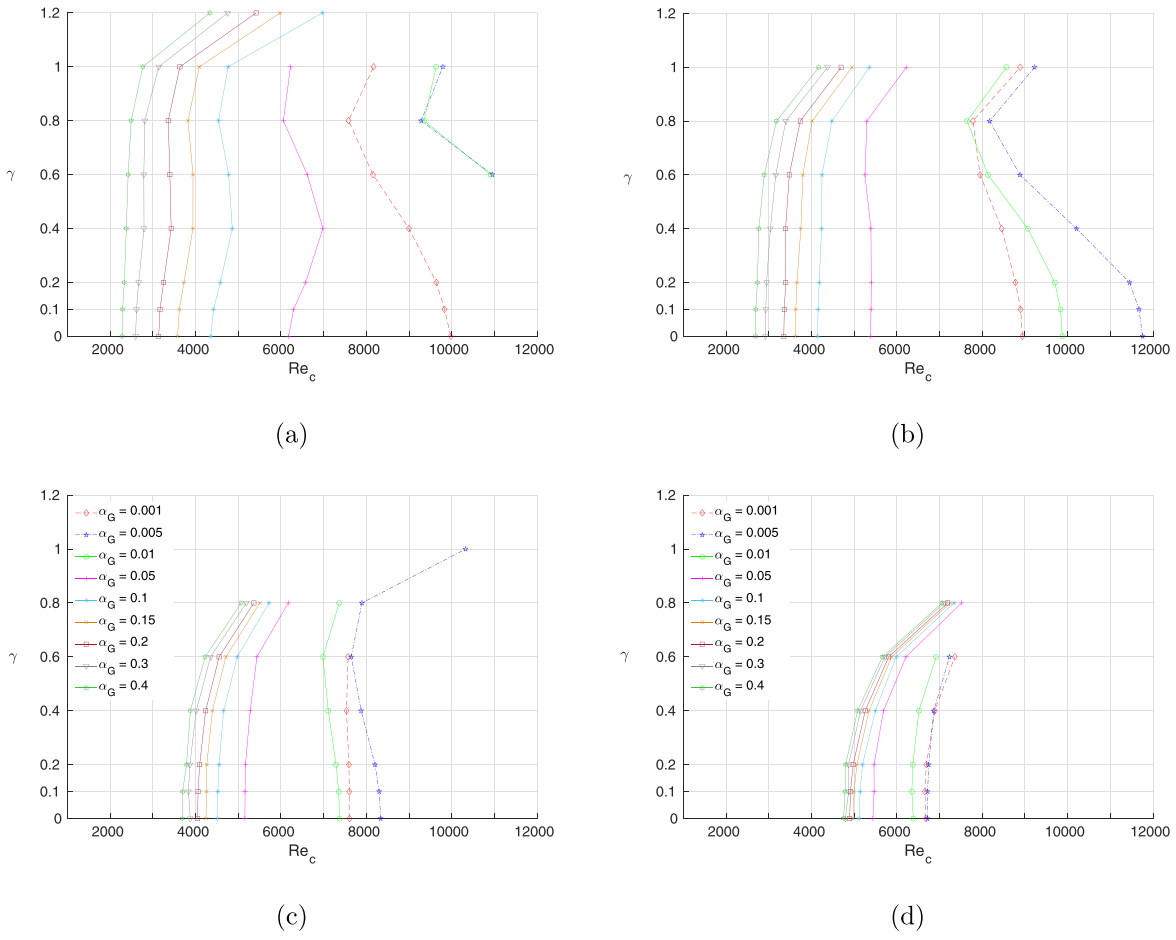

FIG. 12. Critical Reynolds number for three-dimensional disturbances for different values of γ and α_G for $Wi = 6$, for (a) $\beta = 0.125$, (b) $\beta = 0.25$, (c) $\beta = 0.5$, and (d) $\beta = 0.75$.

$Wi = 6$ [Fig. 8(b)], the critical Reynolds for these disturbances is above 12 000. However, for $Wi = 2$ [Fig. 8(a)], it is possible to observe that Squire's theorem is not valid for this fluid. Increasing the spanwise wavenumber causes a reduction in the critical Reynolds for the neutral curves of the three-dimensional disturbances. The increase in the spanwise wavenumber causes possible anticipation of the transition, characterizing a destabilizing factor for these flows. This behavior is more pronounced as the Weissenberg number increases. The critical Reynolds number for the two-dimensional disturbances of these flows is above 12 000. However, the critical Reynolds numbers for the three-dimensional disturbances of these flows are $Re_c \approx 9\,285.937$ for $Wi = 6$, $Re_c \approx 9\,320.41$ for $Wi = 8$, and $Re_c \approx 8\,585.16$ for $Wi = 10$.

Therefore, for fluid flows of this viscoelastic model, three-dimensional disturbances can be much more unstable than two-dimensional ones. The same parameters adopted for the two-dimensional analysis were used in the three-dimensional analysis, changing the spanwise wavenumber γ. These results are presented by using the critical Reynolds numbers. To standardize and make it easier to understand the graphs, for the different values of the Giesekus model parameter α_G, the colors used for these two-dimensional curves in Fig. 3 were kept.

2. Eigenfunction analysis

The eigenfunction for the data in 4 and 5 lines of Table II are shown in Figs. 9 and 10, respectively. These choices correspond to stable and unstable results, respectively. The eigenfunction of the velocity components and the pressure are normalized by the maximum absolute value of the eigenfunction u. The eigenfunction of the extra-stress tensor components are normalized by the maximum absolute value of the T_{xx} eigenfunction. The eigenfunctions of the velocity components and the pressure are shown in Figs. 9(a) and 10(a), respectively. The eigenfunctions of the extra stress tensor components are shown in Figs. 9(b) and 10(b), respectively.

The streamwise and spanwise velocity disturbance eigenfunctions are higher near the walls, where the streamwise base flow velocity gradients and the shear stresses and shear strain are higher and correspond to the region where the fluid stretching is also highest. At the wall, the extra stress tensor is at its maximum value, decaying toward the center

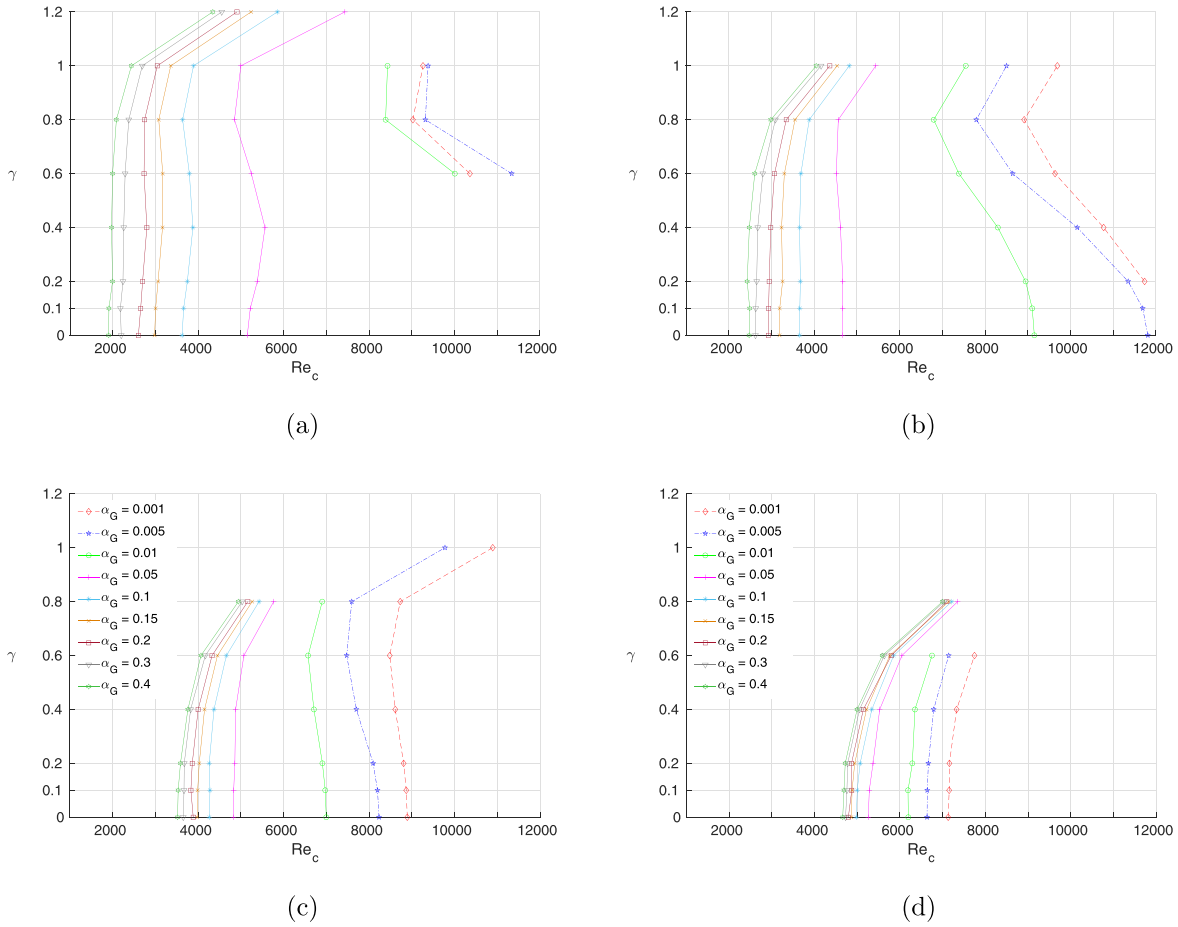

FIG. 13. Critical Reynolds number for three-dimensional disturbances for different values of γ and α_G for $Wi = 8$, for (a) $\beta = 0.125$, (b) $\beta = 0.25$, (c) $\beta = 0.5$, and (d) $\beta = 0.75$.

where the streamwise velocity gradients go to zero. These results show a strong relation between shear and non-Newtonian behavior.

The maximum values of the streamwise eigenfunctions are very close to the critical layer y_c, where the wave speed c matches the base flow streamwise velocity $U(y_c)$. These values are $y = \pm 0.851$ and $y = \pm 0.878$ for the cases shown in Figs. 9 and 10, respectively.

The wave speed variation with β [see Fig. 7(b)] increases significantly when β increases from 0.125 to 0.25. This corresponds to a shift of the critical layer away from the wall.

3. Three-dimensional disturbance critical Reynolds analysis

Figure 11 presents the variation of the critical Reynolds number for different values of the Giesekus model, considering $Wi = 2$, for $\beta = 0.125, 0.25, 0.5$, and 0.75.

It is worth noting that some flows do not have points for spanwise wavenumbers. This is because, for these wavenumbers, stabilization has caused the critical Reynolds to shift to values above 12 000.

Figure 11, for the same values of β analyzed in the last figure, shows that, as the Newtonian contribution in the fluid mixture increases, the range of values for critical Reynolds decreases. In other words, for high β values, α_G has a more limited influence on Re_c. This result shows the influence of the polymer viscosity on the stability of the flow and was also observed for two-dimensional disturbances presented in Figs. 3–6. The influence of α_G is reduced by the polymer viscosity and elasticity.

To analyze the influence of elasticity under the three-dimensional disturbances and its stabilizing/destabilizing effect, Figs. 12–14 present the variation of the Reynolds number, considering Weissenberg number equal to 6, 8, and 10, respectively. The values of β shown in these figures are $\beta = 0.125$, $\beta = 0.25$, $\beta = 0.5$, and $\beta = 0.75$.

For three-dimensional disturbances, it becomes evident that Squire's theorem is not valid for the Giesekus model, for which α_G is associated with anisotropy effects. Figures 12–14 show that, for low values of α_G, increasing three-dimensionality may result in lower critical Reynolds numbers. As α_G or β increases, three-dimensional waves tend to be more and more stable than two-dimensional waves. The

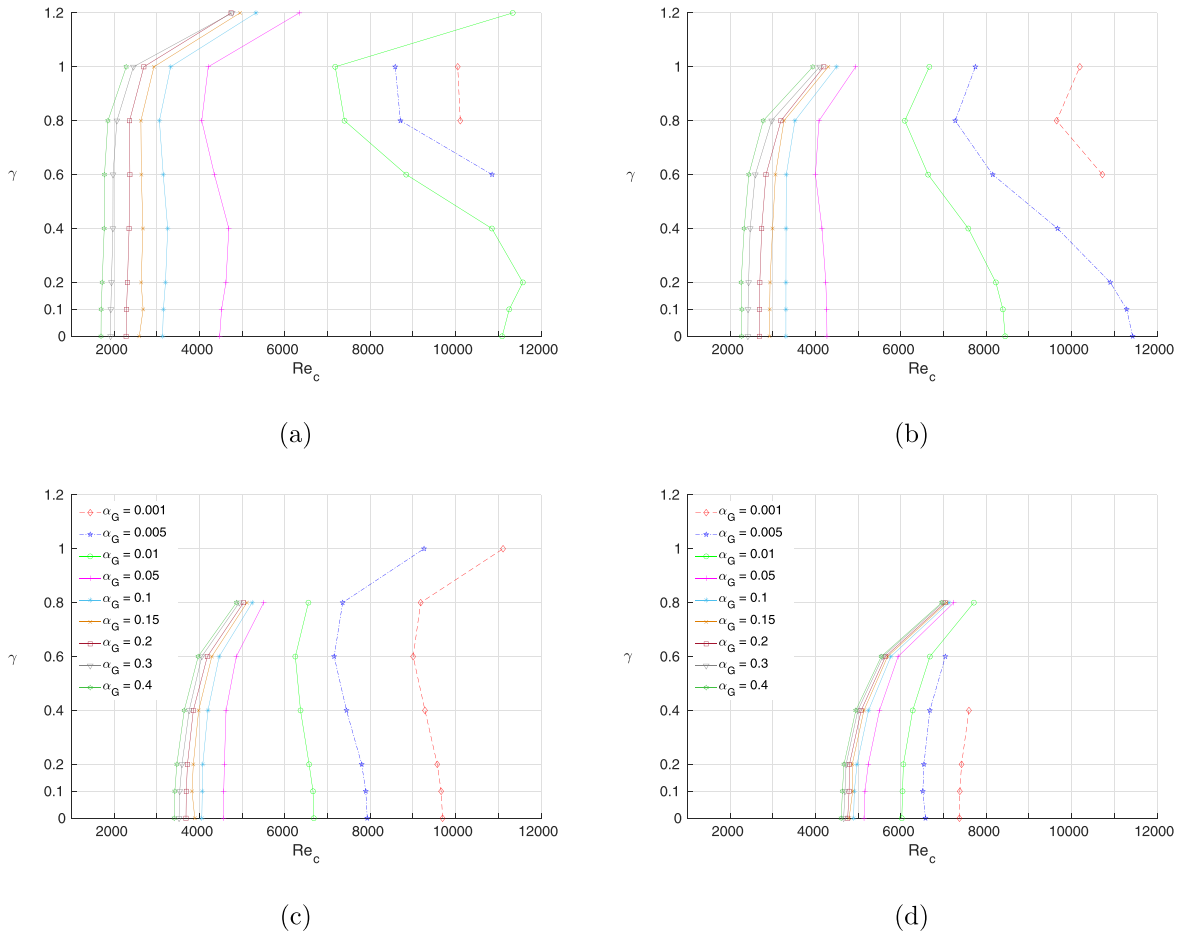

FIG. 14. Critical Reynolds number for three-dimensional disturbances for different values of γ and α_G for $Wi = 10$, for (a) $\beta = 0.125$, (b) $\beta = 0.25$, (c) $\beta = 0.5$, and (d) $\beta = 0.75$.

result is somewhat unexpected since higher values of α_G correspond to higher anisotropy, which is the main reason to contradict Squire's theorem.

As the Weissenberg number increases, three-dimensional disturbances become more predominant in flow's destabilization. Even with the solvent contribution increase, which has the characteristic of stabilization, it is possible to observe a reduction of the critical Reynolds value for $\beta = 0.5$, showing that the three-dimensional disturbances remain more unstable than the two-dimensional ones. This shows the influence of the effect of elasticity on flow stability. Higher elasticity in the viscoelastic fluid means a significant influence of three-dimensional disturbances on flow stability. If combined with low values for the parameter α_G and with high polymer viscosity in the mixture, one can have a reduction in the critical Reynolds value from ≈11 000 considering two-dimensional disturbances to ≈7000 considering $\gamma = 1$ [Fig. 14(a)] for the same flow.

IV. CONCLUSION

This work presents a linear stability analysis for viscoelastic fluid flows to non-stationary disturbances. The constitutive equation for the Giesekus model (3) was used as the viscoelastic model. The fluid flow adopted was incompressible, isothermal viscoelastic flow between parallel plates. In the present work, only the spatial analysis was performed. The adopted method was verified by comparing the results obtained using the present formulation with the work of Blonce,[22] showing an excellent agreement.

The results explore the influence of the parameter α_G of the Giesekus model over the flow stability. It could be verified that small values for this parameter stabilize the flow, increasing the value of the critical Reynolds number. However, as this parameter increases, the opposite effect is verified, becoming a destabilizing factor in the flow. These characteristics are intensified with the increase in the Weissenberg number and when considering higher polymer viscosity in the fluid mixture. These characteristics are valid for both two- and three-dimensional disturbances.

Furlan *et al.*[27] presented a theoretical study on the validity of Squire's theorem for viscoelastic fluid models. That study has shown the validity of Squire's theorem for isotropic non-Newtonian models. On the other hand, for anisotropic models, both DNS and LST results show that Squire's theorem is not valid. Therefore, the numerical results presented in this work support the theoretical study by Furlan *et al.*[27]

The results show that low values of α_G associated with low values of β and high values of Wi result in three-dimensional disturbances that are more unstable than two-dimensional disturbances. It shows that, in this case, Squire's theorem is not applicable. As α_G increases, two-dimensional disturbances tend to be more critical than three-dimensional disturbances, and as β and Wi increase, the destabilizing effect of anisotropy is reduced.

ACKNOWLEDGMENTS

The authors thank Professor André V. G. Cavalieri for the fruitful discussion in developing the LST code.

This study was financed in part by the Coordenação de Aperfeiçoamento de Pessoal de Nível Superior-Brasil (CAPES)-Finance Code 001.

The research was carried out using the computational resources of the Center for Mathematical Sciences Applied to Industry (CeMEAI), funded by FAPESP, Brazil (Grant No. 2013/07375-0).

AUTHOR DECLARATIONS

Conflict of Interest

The authors have no conflicts to disclose.

Author Contributions

Laison Junio da Silva Furlan: Data curation (equal); Formal analysis (equal); Investigation (equal); Methodology (equal); Resources (equal); Validation (equal); Writing – original draft (equal); Writing – review & editing (equal). **Matheus Tozo Araujo:** Data curation (equal); Formal analysis (equal); Investigation (equal); Methodology (equal); Resources (equal); Validation (equal); Writing – original draft (equal); Writing – review & editing (equal). **Marcio T. Teixeira de Mendonca:** Formal analysis (equal); Methodology (equal); Supervision (equal); Writing – original draft (equal); Writing – review & editing (equal). **Analice Costacurta Brandi:** Conceptualization (equal); Formal analysis (equal); Methodology (equal); Validation (equal); Writing – original draft (equal); Writing – review & editing (equal). **Leandro Franco de Souza:** Conceptualization (equal); Formal analysis (equal); Investigation (equal); Supervision (equal); Writing – review & editing (equal).

DATA AVAILABILITY

The data that support the findings of this study are available from the corresponding author upon reasonable request.

APPENDIX: MATRIX METHOD

The matrix method consists of rewriting the system of equations (4)–(13) in the form

$$LV = \alpha FV, \tag{A1}$$

with the eigenvector V defined as

$$V = [u, \alpha u, v, \alpha v, w, \alpha w, p, T_{xx}, T_{xy}, T_{xz}, T_{yy}, T_{yz}, T_{zz}]^T. \tag{A2}$$

Here, the mathematical manipulation required for this solution method is presented.

The matrix system is rewritten in such a way that each row of the matrix corresponds to an equation of the system (4)–(13), and the addition of three rows is required to make the system closed and the matrices square. The matrices L and F have the coefficients for the disturbances in the eigenvector V.

We are defining the matrix L [left-hand side of the system—Eq. (A1)] and the matrix F [right-hand side of the system—Eq. (A1)] in the form with the subindexes (i, j) of $L_{i,j}$ and $F_{i,j}$ denoting row and column, respectively.

For consistency and familiarity with the subindex notation, we rewrite the eigenvector (A2) as follows:

$$V = [V_1, V_2, V_3, V_4, V_5, V_6, V_7, V_8, V_9, V_{10}, V_{11}, V_{12}, V_{13}]^T. \tag{A3}$$

For the first line $i = 1$, the continuity equation [Eq. (4)] is rewritten in the form

$$L_{1,3} * V_3 + L_{1,5} * V_5 = \alpha F_{1,1} * V_1, \tag{A4}$$

with

$$L_{1,3} = Dy,$$
$$L_{1,5} = i\gamma \mathbf{I},$$

and

$$F_{1,1} = -i\mathbf{I}.$$

It is worth noting that each element of the matrices L and F is square matrices with dimension $n \times n$, with n being the number of Chebyshev modes used to approximate the derivatives by polynomials; the term Dy is the Chebyshev matrix for the first derivative, and $Dy2$ is the Chebyshev matrix for the second derivative. All other elements for both matrices in this row are null.

The second line, $i = 2$, is one of the lines included in the system so that the matrices L and F are square, so in that line, we have

$$L_{2,2} * V_2 = \alpha F_{2,1} * V_1, \tag{A5}$$

with $L_{2,2} = F_{2,1} = \mathbf{I}$.

For $i = 3$, the momentum equation in the x direction [Eq. (5)] is rewritten as

$$L_{3,1} * V_1 + L_{3,3} * V_3 + L_{3,9} * V_9 + L_{3,10} * V_{10} = \alpha(F_{3,1} * V_1 + F_{3,2} * V_2 + F_{3,7} * V_7 + F_{3,8} * V_8), \tag{A6}$$

with

$$L_{3,1} = -i\omega_t \mathbf{I} - \frac{\beta}{Re}(Dy2 - \gamma^2 \mathbf{I}), \quad L_{3,3} = \frac{dU}{dy},$$
$$L_{3,9} = -Dy, \quad L_{3,10} = -i\gamma \mathbf{I},$$
$$F_{3,1} = -iU, \quad F_{3,2} = -\frac{\beta}{Re}\mathbf{I},$$
$$F_{3,7} = -i\mathbf{I}, \quad F_{3,8} = i\mathbf{I}.$$

For $i = 4$, the procedure is the same as for the row $i = 2$,

$$L_{4,4} * V_4 = \alpha F_{4,3} * V_3, \tag{A7}$$

with $L_{4,4} = F_{4,3} = \mathbf{I}$.

For $i = 5$, the momentum equation in the y direction [Eq. (6)] is rewritten as

$$L_{5,3} * V_3 + L_{5,7} * V_7 + L_{5,11} * V_{11} + L_{5,12} * V_{12} = \alpha(F_{5,3} * V_3 + F_{5,4} * V_4 + F_{5,9} * V_9), \tag{A8}$$

with

$$L_{5,3} = -i\omega_t \mathbf{I} - \frac{\beta}{Re}(Dy2 - \gamma^2 \mathbf{I}), \quad L_{5,7} = Dy,$$
$$L_{5,11} = -Dy, \quad L_{5,12} = -i\gamma \mathbf{I},$$
$$F_{5,3} = -iU, \quad F_{5,4} = -\frac{\beta}{Re}\mathbf{I}, \quad F_{5,9} = i\mathbf{I}.$$

For $i = 6$, the procedure is the same as for the rows $i = 2$ and $i = 4$,

$$L_{6,6} * V_6 = \alpha F_{6,5} * V_5, \tag{A9}$$

with $L_{6,6} = F_{6,5} = \mathbf{I}$.

For the line $i = 7$, the momentum equation in the z direction [Eq. (7)] is rewritten as

$$L_{7,5} * V_5 + L_{7,7} * V_7 + L_{7,12} * V_{12} + L_{7,13} * V_{13} = \alpha(F_{7,5} * V_5 + F_{7,6} * V_6 + F_{7,10} * V_{10}), \tag{A10}$$

with

$$L_{7,5} = -i\omega_t \mathbf{I} - \frac{\beta}{Re}(Dy2 - \gamma^2 \mathbf{I}), \quad L_{7,7} = i\gamma \mathbf{I},$$
$$L_{7,12} = -Dy, \quad L_{7,13} = -i\gamma \mathbf{I},$$
$$F_{7,5} = -iU, \quad F_{7,6} = -\frac{\beta}{Re}\mathbf{I}, \quad F_{7,10} = i\mathbf{I}.$$

For $i = 8$, the constitutive equation for the tensor T_{xx} [Eq. (8)] is rewritten as

$$L_{8,1} * V_1 + L_{8,3} * V_3 + L_{8,8} * V_8 + L_{8,9} * V_9 = \alpha(F_{8,1} * V_1 + F_{8,8} * V_8), \tag{A11}$$

with

$$L_{8,1} = -2WiTb_{xy}Dy, \quad L_{8,3} = Wi\frac{dTb_{xx}}{dy},$$
$$L_{8,8} = \mathbf{I} - i\omega_t Wi\mathbf{I} + 2\frac{ReWi\alpha_G}{(1-\beta)}Tb_{xx},$$
$$L_{8,9} = -2Wi\frac{dU}{dy} + 2\frac{ReWi\alpha_G}{(1-\beta)}Tb_{xy},$$
$$F_{8,1} = 2iWiTb_{xx} + 2i\frac{(1-\beta)}{Re}\mathbf{I}, \quad F_{8,8} = -iWiU.$$

For $i = 9$, the constitutive equation for the tensor T_{xy} [Eq. (9)] is rewritten as

$$L_{9,1} * V_1 + L_{9,3} * V_3 + L_{9,5} * V_5 + L_{9,8} * V_8 + L_{9,9} * V_9 + L_{9,11} * V_{11} = \alpha(F_{9,3} * V_3 + F_{9,9} * V_9), \tag{A12}$$

with

$$L_{9,1} = -WiTb_{yy}Dy - \frac{(1-\beta)}{Re}Dy, \quad L_{9,3} = Wi\frac{dTb_{xy}}{dy},$$
$$L_{9,5} = i\gamma WiTb_{xy}, \quad L_{9,8} = \frac{ReWi\alpha_G}{(1-\beta)}Tb_{xy},$$
$$L_{9,9} = \mathbf{I} - i\omega_t Wi\mathbf{I} + \frac{ReWi\alpha_G}{(1-\beta)}\left(Tb_{xx} + Tb_{yy}\right),$$
$$L_{9,11} = -Wi\frac{dU}{dy} + \frac{ReWi\alpha_G}{(1-\beta)}Tb_{xy},$$
$$F_{9,3} = iWiTb_{xx} + i\frac{(1-\beta)}{Re}\mathbf{I}, \quad F_{9,9} = -iWiU.$$

For $i = 10$, the constitutive equation for the tensor T_{xz} [Eq. (10)] is rewritten as

$$L_{10,1} * V_1 + L_{10,5} * V_5 + L_{10,10} * V_{10} + L_{10,12} * V_{12} = \alpha(F_{10,5} * V_5 + F_{10,10} * V_{10}), \tag{A13}$$

with

$$L_{10,1} = -i\gamma\frac{(1-\beta)}{Re}\mathbf{I}, \quad L_{10,5} = -WiTb_{xy}Dy,$$
$$L_{10,10} = \mathbf{I} - i\omega_t Wi\mathbf{I} + \frac{ReWi\alpha_G}{(1-\beta)}Tb_{xx},$$
$$L_{10,12} = -Wi\frac{dU}{dy} + \frac{ReWi\alpha_G}{(1-\beta)}Tb_{xy},$$
$$F_{10,5} = iWiTb_{xx} + i\frac{(1-\beta)}{Re}\mathbf{I}, \quad F_{10,10} = -iWiU.$$

For $i = 11$, the constitutive equation for the tensor T_{yy} [Eq. (11)] is rewritten as

$$L_{11,3} * V_3 + L_{11,9} * V_9 + L_{11,11} * V_{11} = \alpha(F_{11,3} * V_3 + F_{11,11} * V_{11}), \tag{A14}$$

with

$$L_{11,3} = Wi\frac{dTb_{yy}}{dy} - 2WiTb_{yy}Dy - 2\frac{(1-\beta)}{Re}Dy,$$
$$L_{11,9} = 2\frac{ReWi\alpha_G}{(1-\beta)}Tb_{xy},$$
$$L_{11,11} = \mathbf{I} - i\omega_t Wi\mathbf{I} + 2\frac{ReWi\alpha_G}{(1-\beta)}Tb_{yy},$$
$$F_{11,3} = 2iWiTb_{xy}, \quad F_{11,11} = -iWiU.$$

For $i = 12$, the constitutive equation for the tensor T_{yz} [Eq. (12)] is rewritten as

$$L_{12,3} * V_3 + L_{12,5} * V_5 + L_{12,10} * V_{10} + L_{12,12} * V_{12} = \alpha(F_{12,5} * V_5 + F_{12,12} * V_{12}), \tag{A15}$$

with

$$L_{12,3} = -i\gamma\frac{(1-\beta)}{Re}\mathbf{I},$$
$$L_{12,5} = -WiTb_{yy}Dy - \frac{(1-\beta)}{Re}Dy,$$
$$L_{12,10} = \frac{ReWi\alpha_G}{(1-\beta)}Tb_{xy},$$
$$L_{12,12} = \mathbf{I} - i\omega_t Wi\mathbf{I} + \frac{ReWi\alpha_G}{(1-\beta)}Tb_{yy},$$
$$F_{12,5} = iWiTb_{xy}, \quad F_{12,12} = -iWiU.$$

Finally, for the line $i = 13$, the constitutive equation for the tensor T_{zz} [Eq. (13)] is rewritten as

$$L_{13,5} * V_5 + L_{13,13} * V_{13} = \alpha F_{13,13} * V_{13}, \tag{A16}$$

with

$$L_{13,5} = -2i\gamma\frac{(1-\beta)}{Re}\mathbf{I},$$
$$L_{13,13} = \mathbf{I} - i\omega_t Wi\mathbf{I},$$
$$F_{13,13} = -iWiU.$$

The boundary conditions imposed no slip and no penetration at the wall, setting u, v, and w equal to zero at these boundaries.

REFERENCES

[1] A. Beris, R. Armostrong, and R. Brown, "Spectral finite-element calculations of the flow of a Maxwell fluid between eccentric rotating cylinders," J. Non-Newtonian Fluid Mech. **22**, 129–167 (1987).
[2] G. Mompean and M. Deville, "Unsteady finite volume of Oldroyd-B fluid through a three-dimensional planar contraction," J. Non-Newtonian Fluid Mech. **72**, 253–279 (1997).
[3] E. Brasseur, M. Fyrillas, G. Georgioou, and M. Crochet, "The time-dependent extrudate-swell problem of an Oldroyd-B fluid with slip along the wall," J. Rheol. **42**, 549–566 (1998).
[4] T. N. Phillips and A. Williams, "Comparison of creeping and inertial flow of an Oldroyd-B fluid though a planar and axisymmetric contraction," J. Non-Newtonian Fluid Mech. **108**, 25–47 (2002).
[5] F. T. Pinho, M. A. Alves, and P. J. Oliveira, "Benchmark solutions for the flow of Oldroyd-B and PTT fluids in planar contractions," J. Non-Newtonian Fluid Mech. **110**, 45–75 (2003).
[6] R. B. Bird, R. C. Armstrong, and O. Hassager, *Dynamics of Polymeric Liquids* (John Willey & Sons, 1987).
[7] H. Giesekus, "Elasto-viskose flüssigkeiten, für die in stationären schichtströmungen sämtliche normalspannungskomponenten verschieden gross sind," Rheol. Acta **2**, 50–62 (1962).
[8] H. Giesekus, "A simple constitutive equation for polymer fluids based on the concept of deformation-dependent tensorial mobility," J. Non-Newtonian Fluid Mech. **11**, 69–109 (1982).
[9] H. Giesekus, "Constitutive equations for polymer fluids based on the concept of configuration-dependent molecular mobility: A generalized mean-configuration model," J. Non-Newtonian Fluid Mech. **17**, 349–372 (1985).
[10] A. A. Draad, G. D. C. Kuiken, and F. T. M. Nieuwstadt, "Laminar–turbulent transition in pipe flow for Newtonian and non-Newtonian fluids," J. Fluid Mech. **377**, 267–312 (1998).
[11] A. Ram and A. Tamir, "Structural turbulence in polymer solutions," J. Appl. Polym. Sci. **8**, 2751–2762 (1964).
[12] D. Samanta, Y. Dubief, M. Holzner, C. Schäfer, A. N. Morozov, C. Wagner, and B. Hof, "Elasto-inertial turbulence," Proc. Natl. Acad. Sci. U. S. A. **110**, 10557–10562 (2013).
[13] H. A. Castillo and H. J. Wilson, "Towards a mechanism for instability in channel flow of highly shear-thinning viscoelastic fluids," J. Non-Newtonian Fluid Mech. **247**, 15–21 (2017).
[14] K.-C. Lee and B. A. Finlayson, "Stability of plane Poiseuille and Couette flow of a Maxwell fluid," J. Non-Newtonian Fluid Mech. **21**, 65–78 (1986).
[15] F. Lim and W. Schowalter, "Pseudo-spectral analysis of the stability of pressure-driven flow of a giesekus fluid between parallel planes," J. Non-Newtonian Fluid Mech. **26**, 135–142 (1987).
[16] R. G. Larson, E. S. G. Shaqfeh, and S. J. Muller, "A purely elastic instability in Taylor–Couette flow," J. Fluid Mech. **218**, 573–600 (1990).
[17] E. S. G. Shaqfeh, S. J. Muller, and R. G. Larson, "The effects of gap width and dilute solution properties on the viscoelastic Taylor–Couette instability," J. Fluid Mech. **235**, 285–317 (1992).
[18] Y. L. Joo and E. S. G. Shaqfeh, "A purely elastic instability in dean and Taylor–Dean flow," Phys. Fluids A: Fluid Dyn. **4**, 524–543 (1992).
[19] R. G. Larson, "Instabilities in viscoelastic flows," Rheol. Acta **31**, 213–263 (1992).
[20] R. Sureshkumar and A. N. Beris, "Linear stability analysis of viscoelastic Poiseuille flow using an Arnoldi-based orthogonalization algorithm," J. Non-Newtonian Fluid Mech. **56**, 151–182 (1995).
[21] M. Avgousti and A. N. Beris, "Non-axisymmetric modes in viscoelastic Taylor–Couette flow," J. Non-Newtonian Fluid Mech. **50**, 225–251 (1993).
[22] L. Blonce, "Linear stability of Giesekus fluid in Poiseuille flow," Mech. Res. Commun. **24**, 223–228 (1997).
[23] J. Mak, "Hydrodynamic stability of Newtonian and Non-Newtonian fluids," Ph.D. thesis (University of Durham, 2009).
[24] M. Zhang, I. Lashgari, T. A. Zaki, and L. Brandt, "Linear stability analysis of channel flow of viscoelastic Oldroyd-B and FENE-P fluids," J. Fluid Mech. **737**, 249–279 (2013).

[25]H. Y. Ye, L. J. Yang, and Q. F. Fu, "Instability of viscoelastic compound jets," Phys. Fluids **28**, 043101 (2016).
[26]A. C. Brandi, M. T. Mendonça, and L. F. Souza, "DNS and LST stability analysis of Oldroyd-B fluid in a flow between two parallel plates," J. Non-Newtonian Fluid Mech. **267**, 14–27 (2019).
[27]L. J. da Silva Furlan, M. T. de Mendonca, M. T. de Araujo, and L. F. de Souza, "On the validity of Squire's theorem for viscoelastic fluid flows," J. Non-Newtonian Fluid Mech. **307**, 104880 (2022).
[28]M. T. Araujo, "Estudo de escoamentos transicionais tridimensionais de fluidos viscoelásticos modelados por giesekus," Ph.D. thesis (Universidade de São Paulo, 2021).
[29]F. Lockett, "On Squire's theorem for viscoelastic fluids," Int. J. Eng. Sci. **7**, 337–349 (1969).
[30]A. M. Grillet, A. C. Bogaerds, G. W. Peters, and F. P. Baaijens, "Stability analysis of constitutive equations for polymer melts in viscometric flows," J. Non-Newtonian Fluid Mech. **103**, 221–250 (2002).
[31]L. J. da Silva Furlan, M. T. de Araujo, A. C. Brandi, D. O. de Almeida Cruz, and L. F. de Souza, "Different formulations to solve the Giesekus model for flow between two parallel plates," Appl. Sci. **11**, 10115 (2021).
[32]H. A. Castillo Sánchez, M. R. Jovanović, S. Kumar, A. Morozov, V. Shankar, G. Subramanian, and H. J. Wilson, "Understanding viscoelastic flow instabilities: Oldroyd-B and beyond," J. Non-Newtonian Fluid Mech. **302**, 104742 (2022).
[33]W. S. Don and A. Solomonoff, "Accuracy and speed in computing the Chebyshev collocation derivative," SIAM J. Sci. Comput. **16**, 1253–1268 (1995).
[34]J. A. Weideman and S. C. Reddy, "A MATLAB differentiation matrix suite," ACM Trans. Math. Software **26**, 465–519 (2000).